ACS APPLIED MATERIALS & INTERFACES

Research Article

www.acsami.org

Effect of Temperature on the Shear-Thickening Behavior of Fumed Silica Suspensions

Justin Warren,[†] Sean Offenberger,[†] Hossein Toghiani,[‡] Charles U. Pittman, Jr.,[§] Thomas E. Lacy,[†] and Santanu Kundu*[,‡]

[†]Department of Aerospace Engineering, [‡]Dave C. Swalm School of Chemical Engineering, and [§]Department of Chemistry, Mississippi State University, MS State, Mississippi 39762, United States

Supporting Information

ABSTRACT: Shear-thickening fluids (STFs) can be subjected to a significant temperature variation in many applications. Polymeric or oligomeric fluids are commonly used as suspending media for STFs. Because the viscosities of polymeric fluids are strongly temperature-dependent, large temperature changes can profoundly affect the shear-thickening responses. Here, the effect of temperature on the shear-thickening behavior of four low-molecular-weight polymeric glycols/fumed silica suspensions is reported. The dispersed-phase volume fraction, its surface chemistry, and the chemical compositions of the suspending media were varied. These factors influence the viscosity and the interactions between the suspended particles and the suspending media. Fumed silica particles with two different silanol-group surface densities were suspended in the polymeric glycols, where these silanol surface groups formed hydrogen bonds with the suspending media's glycols and internal oxygen atoms. Steady-shear experiments were performed over a temperature range spanning approximately 100 °C. The critical shear rate for the onset of shear thickening decreased with decreasing temperature. The critical shear rates were inversely proportional to the viscosity of the pure suspending media over these same temperature ranges. The response of STFs to varying both the temperature and shear rate investigated here will help to design application-specific STFs. Mitigation of a hypervelocity (6.81 km/s) impact on an aluminum facesheet sandwich composite filled with one of these STFs was demonstrated.

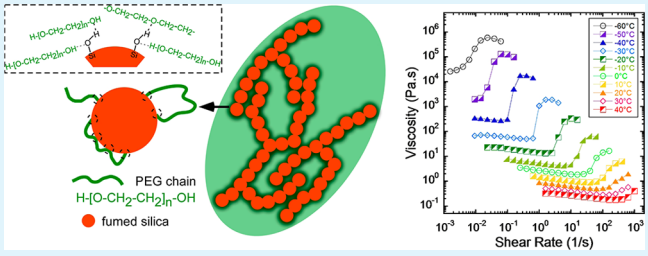

KEYWORDS: *shear-thickening fluids, fumed silica, PEG, rheology, micrometeoroid shielding*

INTRODUCTION

Shear-thickening fluids (STFs) stand apart from other suspensions because of their remarkable shear-rate-dependent behavior. Beyond a critical applied shear rate, the viscosity of a STF increases rapidly, often by several orders of magnitude.[1−4] This rapid increase in the viscosity has been exploited in novel applications such as improving the ballistic impact resistance of soft-body armor[2,5] and vibration damping of alpine skis[6] as well as in spacecraft shielding concepts for mitigating highly energetic micrometeoroid/orbital debris (MMOD) impacts.[7]

The effectiveness of STFs in mitigating high-energetic particle impacts is presented in Figure 1. Here, two 10.16 cm × 10.16 cm aluminum facesheet sandwich composites with 1.27-cm-thick aluminum honeycomb cores are shown after being impacted with a 1-mm-diameter steel sphere (mass of 4 mg) traveling at 6.81 km/s (kinetic energy of 92.75 J). The central portion of the core of the specimen (target) shown in Figure 1 (top) was filled with poly(ethylene glycol) of molecular weight of 200 g/mol (PEG 200), while the central portion of the specimen in Figure 1 (bottom) was filled with a STF nanoparticles consisting of 0.3 mass fraction (MF) Aerosil 200 fumed silica nanoparticles (A200 silica) in PEG 200. Note that there is both a larger volume of core damage and rear facesheet penetration in the PEG 200-filled target versus the STF-filled target. The STF-filled target sustained less core damage and no rear facesheet perforation. Because STFs show promise in mitigating high-energy impacts, these fluids might be useful as a supplementary component to MMOD shielding concepts. STFs suitable for these applications are required to have low solid volume fractions for weight reduction and display shear-thickening responses over a wide temperature range because the surface temperature of spacecraft structures can fluctuate over ±100 °C.

STFs consist of a particulate phase dispersed in suspending media. The interaction between the particles and the suspending media can be varied by selecting particles of different shapes, sizes, and surface chemistries to obtain a large variety of application-specific STFs. However, the mechanistic understanding of the shear-thickening behavior required to design STFs for MMOD shielding applications from such a large parametric space is still incomplete. Further understanding of the effect of the temperature on the shear-

Received: June 9, 2015
Accepted: August 3, 2015
Published: August 3, 2015

ACS Publications © 2015 American Chemical Society

DOI: 10.1021/acsami.5b05094
ACS Appl. Mater. Interfaces 2015, 7, 18650−18661

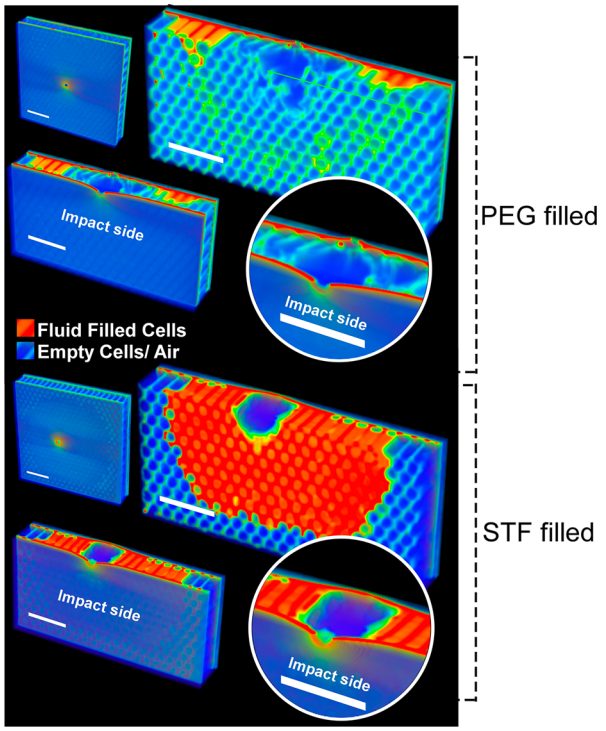

Figure 1. Three-dimensional renderings of computed tomography scans of aluminum facesheet/aluminum honeycomb core sandwich panels each impacted with a 1-mm-diameter steel sphere (mass of 4 mg) at 6.81 km/s (kinetic energy of 92.75 J): (top) central portion of the core filled with PEG 200; (bottom) central portion of the core filled with a STF consisting of 0.3 MF A200 silica in PEG 200. (Note: White scale bars are 20 mm in length.)

thickening behavior is limited. Previous studies of temperature variation were confined in both their scope and temperature range.[8−10]

Several mechanisms have been associated with shear thickening in the literature: (i) an order−disorder transition,[11,12] wherein the alignment of suspended particles in ordered arrays at lower shear rates is disrupted by flow instabilities at higher shear rates, leading to a disordered structure; (ii) dilatancy in high-volume-fraction suspensions similar to that observed in granular solids[3] requiring the interstitial space between close-packed particles to increase in order for particles to move past one other; (iii) the formation of transient particle aggregates defined as hydroclusters.[2,13−15] Additionally, frictional contact between rough particles has been shown to play an important role in certain classes of suspensions.[16−21] Each mechanism involves particle movements, and the presence of one mechanism does not preclude or require the presence of another. The shear-thickening response of a STF is dependent on the particular characteristics of that system. As the particles move, the interactions between the particles and between particles and suspending media change. These changes will be a function of the shear rate and temperature. Several interactions are of interest, for example, van der Waals, electrostatic, steric, frictional, hydrodynamic, and Brownian. These interactions contribute to a complex balance of forces that can lead to transient cluster formations and/or frictional contacts. The formation of these so-called hydroclusters corresponds to a marked increase of the viscosity. Evidence of hydrocluster formation has been observed in small-angle neutron scattering (SANS),[14] and the present study also indicates that hydrodynamics play an important role in the shear-thickening behavior.

At low applied shear rates, the viscosities of many STFs will initially decrease (i.e., shear-thinning behavior) as the at-rest microstructure is disrupted.[2] Here, repulsive forces between the particles play an important role. For instance, the presence of a particle surface charge can result in electrostatic repulsive forces that could prevent two particles from coming into close proximity, decreasing the likelihood of shear thickening. Shearing deformation of the suspending media induces hydrodynamic drag forces on the particles. The hydrodynamic drag force, which is proportional to the applied shear rate, causes the particles to translate and rotate.[22] As the shear rate increases, so too does the hydrodynamic drag force, leading to more particle movement and an increased likelihood that particles will approach one another.

At a critical shear rate, the sum of the repulsive forces acting on the particles (electrostatic and steric repulsion, Brownian effects, etc.) is overcome by the sum of the forces acting to bring the particles into close proximity. According to lubrication hydrodynamics, when two particles approach one another, the suspending media between them must be displaced, and the force required to displace this suspending media is a function of the inverse of the distance between particle surfaces.[4,23] This leads to the theoretical lubrication singularity at zero interparticle distance, preventing particle surface-to-surface contact.[4,23] Thus, for particles to come into close proximity at and above the critical shear rate, the hydrodynamic forces must be very high to overcome the lubrication force and any other repulsive forces.[2] However, the distance between the particles is dictated by the repulsive forces acting between them. Once the interparticular distance between two particles is small enough, the two particles will theoretically enter into closed orbits, wherein the two particles cannot be separated unless a separating force equal in magnitude to the force required to bring them together is acted upon them.[2,4] These hydrodynamic lubrication forces cause the formation of hydroclusters.[2,4] As the name suggests, hydroclusters are transient structures of coalesced particles.[4] Simulations have indicated that the number and size of hydroclusters increases with increasing shear rate.[2,13,15] Significant energy is dissipated to bring the particles into close proximity, and as a result, the characteristic viscosity increase of STFs takes place.[2]

However, Zhao and Davis showed that the lubrication singularity as well as closed orbits can be avoided for two spheres approaching in low-Reynolds-number flow if their surfaces are roughened.[24] This can allow particle surface-to-surface contact and, hence, the development of frictional contact forces. Such frictional contact forces have been shown to play an essential role in producing strong shear thickening in concentrated suspensions in both simulations and experiments.[16−21] Mari et al. notes that while hydrodynamic lubrication forces influence the behavior of lower-concentration suspensions, frictional contact forces play a key role in the behavior of highly concentrated suspensions.[16] Interestingly, Heussinger reported shear thickening and cluster formation in simulations of non-Brownian frictional particles where hydrodynamic lubrication forces were intentionally neglected.[18] Furthermore, using confocal microscopy, Lootens et al. observed the formation of ordered (jammed) structure in high-concentration suspensions of roughened particles.[20] Clearly, shear thickening is an intricate phenomenon that can

DOI: 10.1021/acsami.5b05094
ACS Appl. Mater. Interfaces 2015, 7, 18650−18661

be caused by or related to a variety of physical principles that would depend on the characteristics of each particular system.

The mechanisms leading to shear-thickening behavior are best understood for STFs based on spherical suspended particles. Hydrocluster formation involving the irregularly shaped fractal-like fumed silica nanoparticles used in this study likely involves similar controlling principles, but the effects of the shape, aspect ratio, size, volume fraction of the suspended particles, and alignment of the particles during shear are very complex. The inherent roughness of fumed silica particles due to their branched aggregate nature also raises interesting questions concerning friction as well as possible interlocking of particle branches, and this will be postulated later.

Most recent literature on STFs has considered spherical particles, which undergo dramatic shear thickening only at very high particle volume fractions.[3] However, STFs employing irregularly shaped particles, such as fumed silica nanoparticles, can exhibit shear-thickening intensities similar to those of suspensions based on spherical particles but at much lower volume fractions.[25−29] This is beneficial because reducing the suspended particle volume fraction could lead to significant weight savings for many STF applications. In addition, the shear-thickening response can be tailored by modifying the surface of the fumed silica particles with various functional groups. Hence, changes in the chemical functionality of the particle surfaces can be used to tune the particle−liquid interactions when paired with an appropriate choice of suspending media.[26]

Because the motivation of our research is designing a relatively low density STF that could be used as a component in shielding to protect spacecraft from MMOD impacts, fumed silica nanoparticles were chosen as the dispersed phase. We report here the shear-thickening responses and the effect of the temperature on these responses for suspensions of fumed silica nanoparticles, where the MF and surface chemistry of the fumed silica as well as the molecular weight and architecture of the suspending media were varied. The present theoretical understanding of shear thickening based on hard-sphere suspensions cannot be applied to fumed silica suspensions directly, but an attempt has been made here to explore the complex underlying contributions of the various factors leading to shear thickening. Experiments were conducted over temperature ranges spanning approximately 100 °C. The critical shear rate marking the onset of shear thickening was found to be inversely proportional to the viscosity of the pure suspending media over the temperature range investigated. This shear thickening was attributed to hydrocluster formation caused by the balance of hydrodynamic, steric, frictional, and thermal forces that govern particle interactions.

MATERIALS AND METHODS

Two types of fumed silica nanoparticles and three low-molecular-weight oligomeric glycols (suspending media) were selected to generate the four STFs produced for this study. These suspending media included hydroxyl-terminated poly(ethylene glycol) of molecular weight of 200 g/mol (PEG 200) and of molecular weight of 400 g/mol (PEG 400) and a three-armed glycerol poly(propylene oxide) having a molecular weight of 700 g/mol (PPG 700). Two types of fumed silica nanoparticles were selected: Aerosil 200 (A200 silica) and Aerosil R812 (R812 silica) (Evonik Industries).

A200 and R812 fumed silica nanoparticles consist of approximately spherical SiO_2 primary particles fused together during a flame hydrolysis manufacturing process to form irregularly shaped branched aggregates.[30] The A200 and R812 particles have different surface functional groups (discussed later), so they will interact differently with the suspending media, and the corresponding temperature-dependent shear-thickening behavior will be different. Representative transmission electron microscopy (TEM) images of A200 and R812 silica are shown in parts A and B of Figure 2, respectively. TEM images

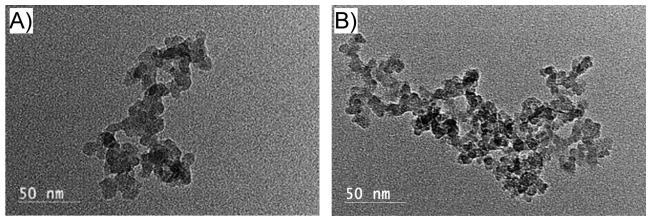

Figure 2. Representative TEM micrographs of (A) A200 silica, displaying the aggregates formed of ≈12-nm-diameter spherical SiO_2 fused primary particles and (B) R812 fumed silica nanoparticle aggregates with ≈7-nm-diameter spherical SiO_2 primary particles. (Note: Image B very likely consists of two to three agglomerated nanoparticles.)

of fumed silica particles were captured using a JEOL 2100 200 kV microscope. Dilute solutions of fumed silica particles in ethanol were deposited on carbon-coated copper grids. Excess ethanol was dried before TEM experiments. On the basis of the literature[30−32] and TEM data, the A200 primary particle size is ≈12 nm and the characteristic lengths of the aggregates are ≈100−200 nm. The A200 silica particles have a specific surface area of ≈200 m^2/g.[30−32] The R812 silica particles have a ≈260 m^2/g specific surface area, and the primary particle size is ≈7 nm.[30−32] TEM images indicated that R812 particles have a characteristic length similar to that of A200 particles.

The fumed silica particles were dried in an oven at 105 °C for at least 24 h and then dispersed in PEG or PPG using a Silverson L4RT-A high shear mixer. As shown in Table 1, three of the four STFs

Table 1. Shear-Thickening Compositions Prepared and the Temperature Range Studied

silica					
type used	MF	volume fraction	suspending fluid	temperature range (°C)	melting point of suspending media (°C)
A200	0.150	0.0696	PEG 200	−60 to +40	−65
A200	0.225	0.1096	PEG 200	−50 to +40	−65
A200	0.150	0.0699	PEG 400	+10 to +80	6
R812	0.150	0.0641	PPG 700	−40 to +40	−32

produced for this study were PEG suspensions: (i) 0.15 MF A200 silica in PEG 200; (ii) 0.225 MF A200 silica in PEG 200; (iii) 0.15 MF A200 silica in PEG 400; and the fourth STF consists of 0.15 MF R812 silica in PPG 700. All STFs were degassed in a vacuum oven for approximately 1 h to remove air incorporated into these suspensions during the high shear mixing.

Steady-shear rheological experiments on the STFs were conducted using a TA Instruments Discovery Hybrid 2 rheometer with 25-mm-diameter parallel-plate fixtures. The environmental chamber of the rheometer was utilized to conduct experiments over a maximum accessible temperature range for each fluid, as shown in Table 1. The lowest experimental temperature employed was either (i) just above the melting point of the corresponding suspending media or (ii) limited by the maximum torque limit of the instrument because decreasing temperatures caused higher viscosities and rising torque values. The maximum temperature investigated was limited by either (i) the lower torque limit of the instrument or (ii) the loss of low-viscosity samples from the rheometer fixture before achieving the critical shear rate. Additional experiments over a limited temperature range were also performed using a Peltier device, which allowed

DOI: 10.1021/acsami.5b05094
ACS Appl. Mater. Interfaces 2015, 7, 18650−18661

imaging of the free surface of the sample during shearing. All experiments were repeated at least three times.

The PEG and PPG molecular structures are shown in Figure 3. The number of repeat units in Figure 2 for PEG 200 and PEG 400 are $n \approx$ 4 and 8, respectively (Figure 3A). The sum of the repeat units x, y, and z for PPG 700 is ≈10 (Figure 3B). The branched (three-armed star) architecture of PPG 700 results in three terminal hydroxyl groups per molecule as opposed to two for the linear PEG 200 and PEG 400 molecules. The ratio of terminal hydroxyl groups to internal oxygen atoms (ether linkage) for PEG 200, PEG 400, and PPG 700 are approximately 3.5:2, 7.5:2, and 10.5:3. The melting points of the suspending media are −65, +6, and −32 °C, respectively, as provided by the manufacturer.

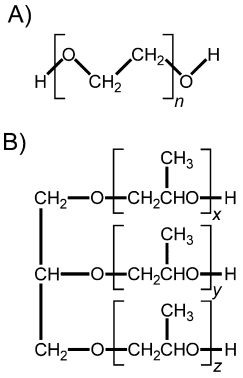

Figure 3. Chemical structures of (A) PEG 200 and 400 and (B) PPG 700.

RESULTS AND DISCUSSION

Shear-Thickening Behavior. Figure 4A displays a representative plot of the average viscosity versus shear rate on a log−log scale for 0.15 MF A200 silica in PEG 200 measured at 20 °C. Initially a shear-thinning behavior is observed for shear rates of approximately 1−100 s^{-1}, wherein the viscosity decreases with increasing shear rate. However, beyond a critical shear rate of approximately 100 s^{-1}, the viscosity increases (i.e., shear thickens) over shear rates of approximately 100−400 s^{-1}. This demonstrates the characteristic attribute of STFs that differentiates them from other suspensions: their viscosity at the higher shear rates can be larger in magnitude than their viscosity at lower shear rates.

In addition to changes in an STF's viscosity, changes in the sample's free surface can also occur with increasing shear rate. Images of the 0.15 MF A200 silica in PEG 200 sample's free surface taken at three important conditions of a rheological experiment are shown as insets in Figure 4A. These images were captured (from left to right) (i) during shear thinning, (ii) near the critical shear rate, and (iii) during advanced shear thickening (corresponding data points are shown by arrows). Interestingly, the free surface of the sample displayed no visible change at the critical shear rate. However, as the shear thickening developed, instabilities formed on the free surface (image corresponding to the highest shear rate in Figure 4A). These instabilities eventually caused a portion of the sample to be ejected, limiting the magnitude of the viscosity increase that could be studied. The loss of sample reduced the torque required to maintain the shear rate, resulting in a decrease in the apparent viscosity not representative of the true STF viscosity. Surface instabilities can be caused by many factors.[33] Here, they are thought to be related to the hydrocluster formation mechanism occurring during the shear-thickening process. The critical shear rate and associated critical shear stress marking the onset of shear-thickening behavior were calculated by determining the point at which the slope changes on the shear stress versus shear rate curve plotted on a log−log scale, as shown in Figure 4B.[8]

Experimental Results. Steady-shear rheological data (i.e., viscosity versus shear rate plotted on log−log scales) for the four STFs considered in this study over the temperature ranges in Table 1 are displayed in Figure 5. Generally, these plots followed the same trends as those discussed for the viscosity versus shear rate curve in Figure 4A. Consider Figure 5A, which displays the viscosity versus shear rate curves for 0.15 MF A200 in PEG 200 over a temperature range of −40 to +40 °C. The curve in Figure 4A is actually the curve marked by solid orange triangles in Figure 5A. Viscosity versus shear rate curves for all experimental temperatures follow the same trends as those discussed above for Figure 4A. For example, the viscosity of the −40 °C curve in Figure 5A (marked by solid blue triangles) decreases over shear rates of approximately 0.01−0.06 s^{-1} (i.e.,

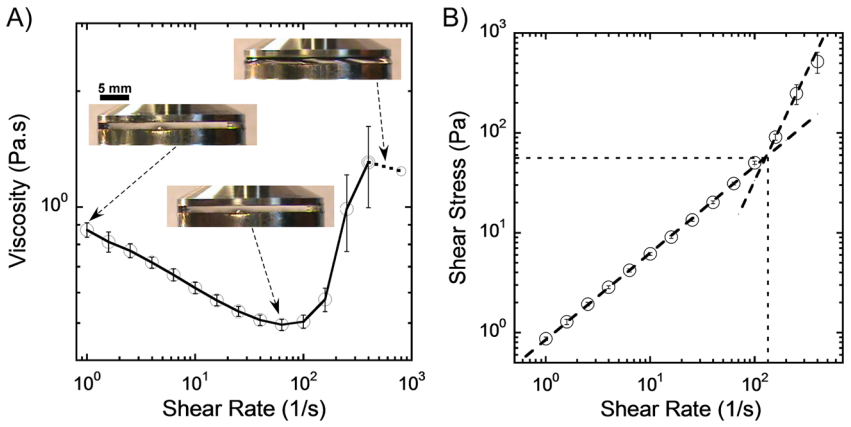

Figure 4. (A) Viscosity versus shear rate for 0.15 MF A200 silica in PEG 200 at 20 °C with images of the sample taken at three key conditions during a steady-shear experiment. The line connecting the points is not a model fit and is provided for visual guidance only. (B) Determination of the critical shear rate and associated shear stress based on the change in the slope of the shear stress versus shear rate curve. (Note: All error bars represent one standard deviation.)

DOI: 10.1021/acsami.5b05094
ACS Appl. Mater. Interfaces 2015, 7, 18650−18661

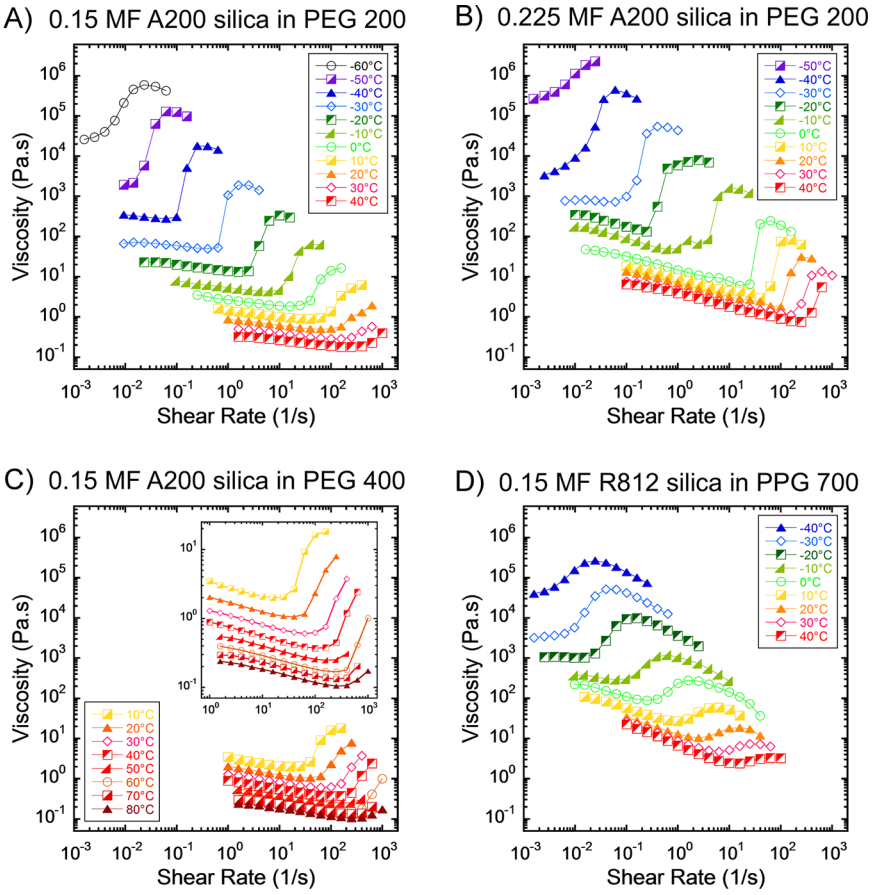

Figure 5. Steady-shear experimental results as a function of temperature for (A) 0.15 MF A200 silica in PEG 200, (B) 0.225 MF A200 silica in PEG 200, (C) 0.15 MF A200 silica in PEG 400 (note: the inset shows the viscosity axis expanded), and (D) 0.15 MF trimethylsilylated R812 fumed silica in PPG 700.

shear thinning) before the viscosity rises markedly (i.e., shear thickening) after a critical shear rate of approximately 0.1 s^{-1}.

Reducing the temperature of an experiment was seen to have four effects on the viscosity versus shear rate curve. First, lowering the temperature of an oligomeric liquid generally increases its viscosity, and this is evident in Figure 5A, where the first few data points of each temperature curve indicate higher initial viscosities as the temperature decreases. Second, lowering the temperature also decreased the critical shear rate; lowering the temperature from +20 to −40 °C reduced the critical shear rate from approximately 100 to 0.1 s^{-1}. Third, as the temperature decreases, the viscosity increases more rapidly following the critical shear rate (i.e., the steepness of the shear-thickening portion of each curve). Last, the overall increase in the magnitude of the viscosity after the critical shear rate increases as the temperature decreases. For example, the viscosity at the critical shear rate for −40 °C (Figure 5A) is approximately 300 Pa·s and rises to a maximum value of around 20000 Pa·s (nearly 2 orders of magnitude), while the increase of the viscosity is approximately 0.5 Pa·s to around 2 Pa·s (less than one order of magnitude) at 20 °C.

The effect of increasing the MF of the suspended particles can be seen by comparing parts A and B of Figure 5. The suspending media was the same for each of these plots (PEG 200), but the MF of A200 silica was increased from 0.15 MF in Figure 5A to 0.225 MF in Figure 5B. Increasing the silica MF from 0.15 to 0.225 in PEG 200 increased the viscosity of the corresponding STFs. For example, the viscosities at a shear rate of 10 s^{-1} at 20 °C (curves marked by solid orange triangles) for 0.15 MF (Figure 5A) and 0.225 MF (Figure 5B) are approximately 0.9 and 7 Pa·s, respectively. Increasing the MF also slightly reduced the critical shear rates. For instance, the critical shear rate at 40 °C (curves marked by half-filled red squares) was approximately 500 s^{-1} for the 0.15 MF sample (Figure 5A), while that of the 0.225 MF sample (Figure 5B) was approximately 200 s^{-1}. Additionally, the viscosity increased more rapidly following the critical shear rate (i.e., the steepness of the shear-thickening portion of the curve) when the MF was increased, which is evident when the 0 °C curves are compared, marked by hollow green circles in Figure 5A,B.

Figure 5C shows the viscosity versus shear rate curves for the 0.15 MF A200 silica in PEG 400 over a temperature range of 10−80 °C. A smaller temperature range could be accurately investigated for the PEG 400 suspension (Figure 5C) because some portions of the samples were ejected from the rheometer geometry early for experimental temperatures above 50 °C.

Increasing the suspending media molecular weight from 200 to 400 g/mol had similar results on the shear rate and temperature-dependent behavior as did increasing the suspended particle MF from 0.15 to 0.225 MF. However, the rheological behavior of the 0.15 MF A200 silica in PEG 400 STF was less shear-rate- and temperature-dependent than the 0.15 MF A200 silica in PEG 200 and 0.225 MF A200 silica in PEG 200 STFs. Recall that PEG 400 has an inherently larger viscosity than PEG 200. Comparing the viscosity at a shear rate of 10 s^{-1} at 20 °C, for the PEG 200-based STF in Figure 5A

DOI: 10.1021/acsami.5b05094
ACS Appl. Mater. Interfaces 2015, 7, 18650−18661

and the PEG 400-based STF in Figure 5C, the viscosity increased from approximately 0.9 to 2 Pa·s because of the higher molecular weight. The critical shear rate decreases slightly for the higher-molecular-weight sample. For example, the critical shear rate at 40 °C was approximately 500 s^{-1} for the PEG 200 sample (Figure 5A), while that of the PEG 400 sample (Figure 5C) was approximately 100 s^{-1}. Comparing the 30 °C curves of Figure 5A,C, the viscosity increased more rapidly following the critical shear rate (i.e., the steepness of the shear-thickening portion of the curve) when the molecular weight of the suspending media was increased.

For the hydrophilic suspended particles (A200 silica) and polar suspending media (PEG 200 or PEG 400), hydrogen bonding is significant (to be discussed later). However, Figure 5D shows the results of experiments for a STF of 0.15 MF R812 silica in PPG 700, where the hydrogen-bonding interactions are much reduced because of the hydrophobic nature of R812 silica, leading to obvious qualitative differences in the shear-thickening behavior compared with the PEG-based STFs in Figure 5A−C.

Note that some trends are similar to those of the PEG-based STFs. The first few data points of each curve show that the viscosity of the STF increases as the temperature falls. Lowering the temperature decreases the critical shear rate. The viscosity increases more rapidly following the critical shear rate (i.e., the steepness of the shear-thickening portion of each curve) at lower temperatures. Although, it is evident from comparing the −10 °C curves marked by green right triangles from Figure 5A,D that the viscosity generally increases less rapidly for the 0.15 MF R812 silica in PPG 700 STF than for a PEG-based STF. Decreasing the temperature leads to larger overall increases in the magnitude of the viscosity after the critical shear rate but not as large an increase in magnitude as the PEG-based STFs, which can be seen by comparing again the −10 °C curves in Figure 5A,D.

One interesting behavior of the 0.15 MF R812 in PPG 700 STF is that the shear thinning before the critical shear rate is more pronounced when the temperature is increased; i.e., the shear-thinning region is steeper with increased temperature. This can be seen by comparing the results for −10 and +40 °C in Figure 5D. Additionally, a pronounced shear-thinning region follows the shear-thickening region of most of the curves in Figure 5D. The surface of the 0.15 MF R812 in PPG 700 STF remained stable over a larger range of shear rates beyond the critical shear rate.

These results indicate that the slope of the viscosity versus shear rate curve changes with the sample composition. Such changes can be qualitatively described as either continuous or discontinuous shear-thickening processes.[3] Continuous shear-thickening represents a gradual increase of the viscosity, whereas a very rapid increase of the viscosity is described as discontinuous shear thickening. The difference between these behaviors can be clearly seen on a viscosity versus shear stress curve by considering the slope of the linear region of the shear-thickening portion of the curve (i.e., portion of curve where the viscosity increases following the shear-thinning region). In general, for discontinuous shear thickening, the slope of the viscosity versus shear stress curve will exceed unity in the shear-thickening regime.[3] Figure 6 shows the viscosity versus shear stress curve for each of the four STFs at 20 °C along with a dashed line with a slope of one. It is clear that all four STFs exhibit continuous shear thickening. However, consider the results for both 0.15 and 0.225 MF A200 in PEG 200 (marked by the green right triangles and blue half-solid squares, respectively). As the silica MF is increased, the shear-thickening slope approaches a value of 1. Thus, the shear thickening approaches a discontinuous behavior. At some silica MFs greater than 0.225 for A200 in PEG 200, the STF would be expected to display discontinuous shear-thickening behavior. Note that the 0.15 MF R812 silica in PPG 700 STF marked by solid black circles in Figure 6, where the hydrogen bonding between the suspended silica particles and the suspending media is reduced compared with the A200-silica-based STFs, displays significantly more continuous behavior than the three PEG-based STFs. The slope of the shear-thickening portions of viscosity versus shear stress plots remained constant with varying temperature for the PEG-based STFs (see Figure S1 in the Supporting Information). However, the corresponding shear-thickening slope of the R812 silica in PPG 700 STF decreased with increasing temperature, becoming progressively more continuous at higher temperatures.

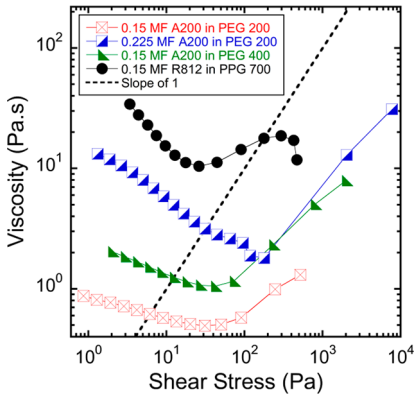

Figure 6. Viscosity versus shear stress for four different STFs at 20 °C along with an arbitrarily placed dashed line with a slope of one. Slope values of the shear-thickening portions of the curves greater than zero indicate shear thickening, and slope values equal to or greater than one are regarded as discontinuous shear thickening.

Surface Chemistry and Solvation Layer. The different shear-thickening behaviors discussed above depend on the suspended particles' morphologies and surface chemistry, which affected the degree to which the suspended particles formed hydrogen bonds with the suspending media, either more hydrogen bonding (A200 silica in PEG 200/400) or less hydrogen bonding (R812 silica in PPG 700). The large silica surface area enables surface functional group interactions with the suspending media to greatly impact how these particles respond to hydrodynamic forces and, hence, their hydrocluster formation.[30,32] The main functional groups present on fumed silica (Figure 7A−C) include isolated silanol groups, bridged silanol groups, and siloxane oxygen atoms.[32] The isolated and bridged silanol group surface densities for A200 silica are ≈1.15 and ≈1.35 nm^{-2}, respectively.[31,32] These hydroxyl groups acidify A200 silica to pH values of 3.7−4.7 and render A200 silica hydrophilic. When A200 silica is dispersed in the PEGs used in this study, hydrogen bonds readily form between the silanol groups on the A200 silica surfaces and PEG.

In contrast to A200 silica, R812 silica is hydrophobic. R812 silica is made from Aerosil 300 (A300 silica; Evonik Industries), which has a specific surface area of ≈300 m^2/g. A300 silica is post-treated with hexamethyldisilazane (Figure 7D), which results in conversion of the isolated silanol groups of A300 silica to trimethylsilyl groups (Figure 7E).[30,31] This marginally

DOI: 10.1021/acsami.5b05094
ACS Appl. Mater. Interfaces 2015, 7, 18650−18661

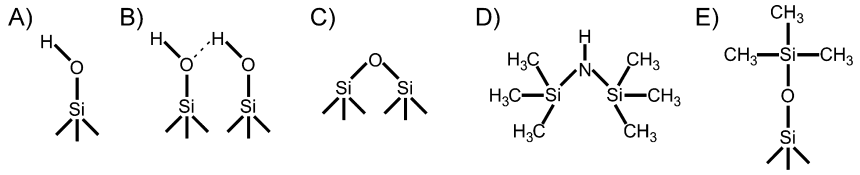

Figure 7. Chemical structures of (A) an isolated silanol group, (B) a bridged silanol group, (C) a siloxane group, (D) hexamethyldisilazane, and (E) a trimethylsilyl surface group.

reduced the surface area of R812 to ≈260 m^2/g. The bridged silanol groups on A300 silica are partially retained on the surface of R812 silica with a surface density of ≈0.44/nm^2 after treatment with hexamethyldisilazane.[32]

In bulk liquid PEG and PPG, hydrogen bonding occurs between hydroxyl-terminated end groups as well as between hydroxyl end groups and internal ether groups. However, the propensity of hydrogen bonding is higher near the fumed silica surfaces (particularly, A200), which have a large number of silanol groups. Silanol groups are more acidic than the terminal hydroxyls of PEG and better hydrogen-bond donors. Figure 8

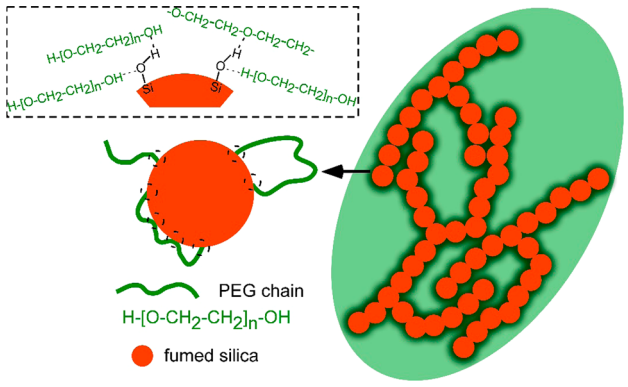

Figure 8. Schematic representation of proposed hydrocluster formation in a fumed silica suspension involving steric interactions between silica particles by hydrogen-bonded liquid solvation layers (dark-green area surrounding the particles). Hydrogen-bonding possibilities between A200 silica and PEG are represented in the inset image. Hydroxyl-terminated PEG ends and an isolated silanol on the particle surface as well as an internal oxygen atom of PEG participate. Both silica and PEG can serve as hydrogen-bond donors and acceptors.

shows several of these hydrogen-bonding possibilities between the suspending media and the silanol groups present on the fumed silica surfaces. Note that all hydrogen bonds are in dynamic equilibrium, rapidly forming and breaking. Multiple hydrogen bonds may exist between individual molecules of PEG (or PPG) and silica, reducing the rate of exchange of these suspending fluid molecules at the surface with bulk fluid. All surface hydrogen bonds between silica and a suspending media molecule must have broken for that molecule to diffuse away from the surface, which is very unlikely. Hydrogen bonding results in the development of a solvation layer near the surface, where the density of oligomeric chains is higher than that of the bulk. As the temperature increases, the rate of dynamic exchange at the surface (the exchange between the solvation layer and the bulk) and the rate of diffusion of oligomer molecules increases. However, the solvation layer is always present at all temperatures investigated here.

The thickness and density of the solvation layer will significantly affect the shear-thickening responses, as is evident when the results plotted for the PEG 200 and PEG 400 suspensions in parts A and C of Figure 5, respectively, are compared. The thickness of the solvation layer will depend on the molecular weight of the oligomeric molecules, chain conformation, and nature of the association between the oligomer chains and surface functional groups.[34−37] The solvation layer thickness was not measured for our systems, but several observations can be made. The estimated number of Kuhn segments (N) for a PEG 200 molecule is less than 2, considering the Kuhn length (b) of 1.1 nm.[38] Thus, it seems unlikely that this molecule will form a loop, where both of the terminal glycol hydroxyl groups form simultaneous hydrogen bonds with the surface. PEG 200 molecules may align themselves along the fumed silica surface, forming −SiOH to ether group hydrogen bonds at one or more locations (Figure 8). Another possibility will be the formation of hydrogen bonds between one terminal glycol hydroxyl and the silanol group at the surface. The fully extended length of the PEG 200 chain is about 1.8 nm, whereas the root-mean-square end-to-end distance ($R_0 = bN^{1/2}$) of a freely jointed PEG 200 chain is approximately 1.3 nm. Similarly, the fully extended chain length of PEG 400 is about 3.8 nm (approximately 3 Kuhn segments), and the root-mean-square end-to-end distance for PEG 400 is close to 1.9 nm. Similar to PEG 200, it is improbable that the PEG 400 chains will adopt and reach a fully extended conformation by hydrogen bonding of only one terminal glycol hydroxyl group to silanol groups (−SiOH) on the surface. Hence, loop formation is possible. Determining the exact conformational distribution and averages of oligomer chains in the surface solvation layer is beyond the scope of this work. However, multiple hydrogen bonds likely exist, on average, between A200 silica and both PEG 200 and PEG 400.

Experimentally, the thickness of the adsorbed PEG layer on spherical silica particles has been estimated to be on the order of 1 nm.[35,36] Recently, He et al. used a magnetophotonic approach to determine the thickness of the solvation layer on silica-coated Fe_3O_4 particles in water and in aqueous mixtures of organic solvents including methanol, ethanol, ethylene glycol (EG), and diethylene glycol (DEG).[39] The solvation layer thickness in water is 4.4 nm, that in 50% methanol is 4.1 nm, and that in 50% ethanol is 3.5 nm. For 50% EG, the thickness is 1.8 nm, which further decreases to about 1.5 nm when the EG concentration was 90%. In comparison to EG, no significant difference was observed for DEG. PEG oligomers used in this study are expected to display behavior similar to that of DEG and EG. On the basis of these results,[35,36,39] the solvation layer thickness for PEG will be between 1 and 2 nm.

R812 silica has a smaller surface density of silanol groups, ≈0.44/nm^2, than A200 silica (≈2.5/nm^2) and no isolated silanols.[32] Thus, R812 silica is less acidic (pH 5.5−7.5) compared to A200 silica (pH 3.7−4.7). Consequently, R812 silica forms fewer hydrogen bonds per unit surface area when dispersed in PEG and PPG because of less favorable hydrogen

DOI: 10.1021/acsami.5b05094
ACS Appl. Mater. Interfaces 2015, 7, 18650−18661

bonding. Steric shielding of some bridged silanol and siloxane groups by bulky trimethylsilyl groups further reduces hydrogen bonding, and it also increases the hydrophobicity. However, R812 silica gel formation (flocculation) in PPG 700 is prevented, in part, because of the small amount of hydrogen bonding that takes place between the particles and the fluid as well as hydrophobic−hydrophobic interactions occurring between the anchored *tert*-butyl groups of the particles and the PPG, which has a lower oxygen-to-carbon ratio than the PEGs.

PPG 700 oligomers are larger than PEG 200 and PEG 400, and thus the solvation layer thickness for PPG 700 could be thicker than those of the PEGs. It is anticipated that, because of fewer hydrogen bonds and nonspecific hydrophobic−hydrophobic interactions, the solvation layer of PPG will be less dense than those of PEG. This is believed to have led to the different viscosity versus shear rate behavior seen when the 0.15 MF A200 silica in PEG 200 results in Figure 5A and the 0.15 MF R812 silica in PPG 700 results in Figure 5D are compared.

Theoretical Analysis. Particle interactions, and, hence, hydrocluster formation and shear-thickening behavior, in these STFs are believed to be governed by a force balance. Different types of interactions are acting on these systems in a complex manner. It is almost impossible to quantify the effect of individual interactions on the shear-thickening responses. This becomes further complicated because some of these interactions are a function of temperature. Here, we attempt to elucidate some of these interactions. As indicated by Raghavan et al.,[26] the Hamaker constants of the fumed silica and suspending media are very similar, particularly for PEG 200, resulting in negligible van der Waals forces. Therefore, van der Waals forces have been neglected from the force balance governing the STFs in this study. It has also been postulated that the van der Waals forces between particles will not be significant and can be neglected in nonaqueous high-particle-concentration systems.[26]

During shearing deformation of suspensions, the relative motion between the suspending media and the particles causes the particles to translate and rotate. As the shear rate increases, so too does the particle movement and the likelihood that two particles will approach one another. This causes a hydrodynamic lubrication force due to the flow of the suspending media out from the gap between two particles. If the particles have entered closed orbits, the force required to separate them is equal in magnitude to the force required to bring them together. These forces are inversely proportional to the separation distance between the particles. The hydrodynamic force has been derived for two spheres approaching along their line of centers by determining the pressure field upon solving the Stokes equation.[40,41] The pressure field can be integrated over the surface of one of the spheres[8,42]

$$F_{\text{hydrodynamic}} = \frac{6\pi\eta_0 a^3\dot{\gamma}}{h} \tag{1}$$

where η_0 is the zero-shear viscosity of the suspending media, a is the particle radius, $\dot{\gamma}$ is the shear rate, and h is the interparticle distance. Equation 1 also describes the force required to separate two particles in close proximity, where the suspending media would flow into the space vacated by the separating particles.

TEM micrographs (Figure 2) demonstrated that fumed silica particles have fractal-like (branched) structures composed of multiple aggregated spherical particles. Therefore, eq 1 cannot be applied directly for fumed silica systems. The corresponding functional form for the fractal-like particles is not known. However, we can assume that $F_{\text{hydrodynamic}}$ will have a functional form somewhat similar to that presented in eq 1, i.e.

$$F_{\text{hydrodynamic}} \sim f\left(\frac{\eta_0 a_c^{\,3}\dot{\gamma}}{h}\right) \tag{2}$$

If a_c is chosen as the hydrodynamic radius of a fumed silica particle and considering that the minimum distance between two nearest particles is equal to twice their hydrodynamic radius, the value of h will be very large, and the corresponding $F_{\text{hydrodynamic}}$ will be small. The repulsive forces would dominate the system, and hydrocluster formation and the corresponding shear thickening would not be significant. However, it is possible that specific segments (or branches) of a fumed silica particle will be near the segments of another particle, while at the same instant, other parts of the particles can be far apart because of their branched nature. In that case, the hydrodynamic force between two segments in the same vicinity becomes important. Here, a_c can be considered as the local radius of curvature of the fumed silica particle, which is related to the radius of the primary particles. It is anticipated that different segments of multiple particles interacting hydrodynamically on a local scale (Figure 8) could contribute to hydrocluster formation.

The interlocking of particle branches might play a role in keeping particles in close proximity, especially for interior particles of developed hydroclusters. Consider two approaching branched particles forming interlocks. Shearing of the suspending media would likely cause the particles to rotate and allow the interlocked branches to separate. However, consider a hydrocluster of many particles. Rotation of some particles, especially interior ones, might be restricted because of the combined interlocking of many particles' branches. This might prolong the coalesced configuration of a hydrocluster, which would be conceptually similar to the theoretical closed orbit of lubrication hydrodynamics that is part of the hydrocluster mechanism concept. The contribution to hydrocluster coalescence and growth due to the interlocking of particle branches would likely be a function of increasing shear rate because of the reliance on interlocking of interior particles of maintaining a hydrocluster configuration.

Recent simulation and experimental studies have reported that once the separation distance between particle surfaces is very small, a frictional contact force would arise proportional to the normal force.[16,19,24] However, in these studies, the presence of a solvation layer, composed of suspending media molecules, present on particles' surfaces was not considered, and the particle volume fractions employed in these studies were much greater than those used with the fumed silica particles in our current work (Table 1). We believe the solvation layer of suspending media present on our fumed silica surfaces because of hydrogen bonding would likely preclude particle surface-to-surface contact, and hence there would not be a frictional contact force in the traditional sense. If such contact occurs, particles, particularly A200, would form hydrogen bonds between themselves, and the particles would remain coalesced because of hydrogen bonding when the shear flow is removed. As a result, the shear-thickening process would be significantly less reversible. Our preliminary results indicate that the shear-thickening responses for the STFs considered here are mostly

DOI: 10.1021/acsami.5b05094
ACS Appl. Mater. Interfaces 2015, 7, 18650−18661

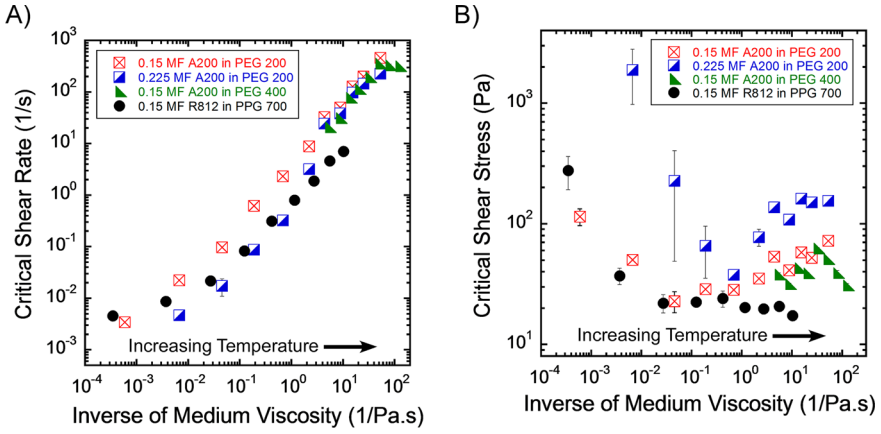

Figure 9. Critical shear rate (A) and shear stress (B) values for four STFs plotted against the inverse of the pure suspending media viscosity for each experimental temperature.

reversible. In a recent study, Liu et al. has shown that gelation due to particle surface-to-surface contacts takes place in STFs with higher concentrations of fumed silica particles that are subjected to elevated temperatures (≈80 °C), where the chain exchange is high.[10] Furthermore, the shear-thickening behavior observed in the present study is mostly continuous. We therefore consider that frictional forces may have some contribution toward the shear-thickening process, but such a contribution is not thought to be dominant.

With regard to repulsive forces, Brownian motion of suspended particles causes the particles to move away from each other. This counteracts hydrocluster formation. The Brownian force arises when the particles diffuse from a sheared configuration to a random configuration. Brownian forces (F_{Brownian}) scale with k_BT/a, where k_B is the Boltzmann constant, T is the temperature of the system, and a is the hydrodynamic radius.

The diffusivity D_0 of a single particle can be written as

$$D_0 = \frac{k_BT}{6\pi\eta_0 a} \tag{3}$$

where a is considered to be the hydrodynamic radius of the fumed silica particles because the branches will not diffuse independently due to stiffness. Importantly, a is quite large for the fumed silica particles considered here, so the corresponding D_0 will be small. The time scale associated with movement of a particle is $\sim a^2/D_0$. Larger a and smaller D_0 values can result in a larger time scale for particle diffusion. As the temperature is reduced, the magnitude of D_0 also decreases. This will result in still slower diffusion at lower temperature. Thus, the suspended fumed silica particles in oligomeric media in these STFs will experience only weak random motions that oppose hydroclustering.

Additionally, as the interparticle distance continues to decrease, a steric repulsive force is postulated to arise because of the compressive interaction of the approaching particles' solvation layers. This repulsive interaction becomes important when the interparticular distance is twice the solvation layer thickness because each particle has such a layer. Vincent et al. developed two repulsive potential functions for two approaching surfaces with strongly anchored polymer steric layers to describe the osmotic mixing of the anchored polymers with the suspending media as well as the elastic compression of the anchored polymers (see eqs S1 and S2 in the Supporting Information).[43] Differentiating the two potential functions with respect to the interparticle distance leads to the force expressions (see eqs S3 and S4 in the Supporting Information). The steric repulsive force when two particles with surface-anchored polymers approach can be given by

$$F_{\text{steric}} = F_{\text{elastic}} + F_{\text{mixing}} \tag{4}$$

If the anchored polymer is considered to be the hydrogen-bonded solvation layer, which is the same composition as the suspending media, the F_{mixing} term can be ignored. On the basis of Vincent's formulation, the steric force can then be written as

$$F_{\text{steric}} \sim \frac{a_c k_B T \delta \phi \rho}{M} g\left(\frac{h}{\delta}\right) \tag{5}$$

where ϕ is the volume fraction of the suspending media contained in the solvation layers (equal to 1 for our case), δ is the solvation layer thickness, ρ is the suspending media density, M is the molecular weight of an oligomer chain of the suspending media, and $g(h/\delta)$ is a nondimensionalized functional form of the interparticle distance, h. The F_{steric} component will be important as h approaches the value of 2δ. Similar surface interaction potentials have been proposed by others.[44,45]

In contrast to Vincent's use of "strongly anchored" polymer chains,[43] the solvation layers of the A200 silica suspensions in PEG 200 and 400 will be composed of dynamically exchanging hydrogen-bonded suspending media only. These oligomers are not permanently covalently anchored. Now, the force required to perturb an ideal polymer chain is given by

$$f = \frac{3k_BT}{Nb^2}R \tag{6}$$

where R is the chain end-to-end distance. Note that the deformation of an ideal polymer chain is represented as a spring, where $3k_BT/Nb^2$ is the entropic spring constant. Interestingly, a chain becomes stiffer with increasing temperature. Now, the polymer chains in the solvation layer will not have their ideal bulk solution distribution of conformations, and there will be small enthalpic effects during compression. However, the force required to compress these chains will have a functional form similar to eq 6, i.e.,

DOI: 10.1021/acsami.5b05094
ACS Appl. Mater. Interfaces 2015, 7, 18650−18661

force ∼ spring constant

× length by which the solvation layer is compressed (7)

Note that eqs 5 and 6 are similar. Therefore, the functional form given in eq 5 can be used for our analysis.

The onset of shear thickening occurs when the sum of all repulsive forces becomes equal to the sum of the forces acting to put and keep particles in close proximity

$$F_{\text{Brownian}} + F_{\text{steric}} \approx F_{\text{hydrodynamic}} + F_{\text{friction}} \quad (8)$$

As discussed above, F_{friction}, which is caused by particle-to-particle contact, is not a major factor, i.e., $F_{\text{friction}} \approx 0$, at least over the temperature range considered here. The force component equations discussed above are simplified based on the interactions between only two particles. In a real system, the interactions between multiple particles would need to be considered. However, the force balance would result in a form dimensionally similar to that given in eq 8.

$$\left[\frac{k_B T}{a} + \frac{a k_B T \delta \phi \rho}{M} g\left(\frac{h}{\delta}\right)\right] \sim f\left(\frac{a_c^3 \eta_0 \dot{\gamma}_c}{h}\right) \quad (9)$$

where $\dot{\gamma}_c$ is the critical shear rate.

This phenomenological relationship (eq 9) can be investigated for the STFs considered in this study. The critical shear rates and associated critical shear stresses were estimated by determining the point at which the slope changes on the shear stress versus shear rate curves, as shown in Figure 4B for each temperature tested. Also, the viscosities of the suspending liquids without dispersed fumed silica were determined at each temperature. For the four STFs considered here, the critical shear rates and associated critical shear stresses determined for each experimental temperature were plotted against the inverse of the pure suspending media's viscosity at that corresponding temperature (Figure 9A,B).

Figure 9A demonstrates that the critical shear rates approximately scaled with the inverse of the viscosities of the pure suspending media, i.e., $\dot{\gamma}_c \sim \eta_0^{-1}$. A deviation from this relationship was observed at lower experimental temperatures. Similar observations have been made by Boersma et al. for various concentrated dispersions[8] but only over a limited temperature range.

The above relationship also indicates that $\dot{\gamma}_c \eta_0$ = critical shear stress = a constant. This can be obtained from the right side of eq 9 and considering that a_c^3/h does not change. However, as shown in Figure 9B, the critical shear stress values vary with the experimental temperature. The critical shear stresses for the PEG 200 and PPG 700 STFs drop rapidly as the reciprocal of the viscosity increases (i.e., the viscosity decreases) and then rise for the two STFs dispersed in PEG 200 as the viscosity decreases further. The critical shear stress values for PPG 700 level out and show no further increase as the viscosity continues to decrease. The critical shear stresses for 0.15 MF silica in PEG 400 do not show a sharp drop as the temperature is increased above the PEG 400 melting point. However, the experimental temperature range was limited for this case.

Near the melting points of PEG 200 and PPG 700, the critical shear stress values are high. It is likely that at those temperatures some kind of local order formation can take place in the suspending media, and because of this networklike structure, the critical shear stress values are high. With increasing temperature, as the viscosity decreases, such ordering disappears. Further increases of the temperature resulted in increasing Brownian force and an increase of the stiffness of the solvation layer. Therefore, a higher force is necessary to bring the particles close together for hydrodynamic coupling. Similar increases in the critical shear stress have been reported by Mewis and Biebaut with an increase in the thickness of the stabilized layer as the temperature is increased.[9] Similar to that study, the critical shear stress values also increase with increasing concentration of suspended particles, which is again linked with the dense solvation layer. As discussed earlier, for the PPG system, the solvation layer is not as dense as those of the PEGs, and the corresponding force to deform the solvation layer does not change significantly with increasing temperature. As a result, the critical stress almost remained constant with increasing temperature.

The above results indicate that the shear-thickening behavior of a fluid can be designed in multiple ways. For instance, the isolated silanol groups of fumed silica can be capped with various functional groups of different lengths and chemical compositions to modify their polarity, hydrogen-bonding character, hydrophobicity, etc. Also, the suspending liquids can be polar or nonpolar, hydrophilic or hydrophobic, and hydrogen-bonding or non-hydrogen-bonding. The liquid can have higher or lower molecular weights, and its viscosity can be varied. All of these factors can tailor the shear-thickening response and will be systematically studied in future publications.

CONCLUSIONS

The temperature-dependent shear-thickening behavior of four STFs consisting of fumed silica and oxygen-containing oligomeric suspending media was investigated. A framework was advanced to support hydrocluster formation as the mechanism behind the shear-thickening behavior for suspensions of fractal-shaped silica particles. Cluster formation is governed by a force balance among hydrodynamic, thermal, steric, and frictional forces.

Shear thickening in these STFs, (i) 0.15 MF A200 silica in PEG 200, (ii) 0.225 MF A200 silica in PEG 200, (iii) 0.15 MF A200 silica in PEG 400, and (iv) 0.15 MF R812 silica in PPG 700, was shown to exist over a temperature range of approximately 100 °C, beginning very near the melting point of suspending media. The critical shear rates marking the onset of shear thickening over the range of temperatures investigated were found to be inversely proportional to the viscosity of the pure suspending media at those same temperatures. Therefore, an expression for the temperature-dependent onset of shear thickening should likely be based on the critical shear rate.

In general, reducing the temperature resulted in lower critical shear rates. Regardless of temperature, increasing the fumed silica MF resulted in lower critical shear rates and increased critical shear stresses. Higher MFs also resulted in behavior closer to that of discontinuous shear thickening. Changing the particle surface chemistry and suspending media architecture (i.e., suspending trimethylsilylated R812 silica in PPG rather than A200 silica in PEG) greatly reduced the hydrogen-bond density formed between the surface of the particles and the suspending media. This resulted in a significantly more continuous shear-thickening behavior. SANS and ultra-small-angle neutron scattering experiments as a function of the shear rate and temperature are underway to discover direct evidence

DOI: 10.1021/acsami.5b05094
ACS Appl. Mater. Interfaces 2015, 7, 18650−18661

of hydrocluster microstructure formation (sizes and shapes) within the STFs.

■ ASSOCIATED CONTENT

Supporting Information

The Supporting Information is available free of charge on the ACS Publications website at DOI: 10.1021/acsami.5b05094.

Viscosity versus shear stress data for four STFs at all temperatures and F_{steric} based on Vincent's formulation (PDF)

■ AUTHOR INFORMATION

Corresponding Author

*E-mail: santanukundu@che.msstate.edu.

Funding

This work was supported by a NASA Space Technology Research Fellowship.

Notes

The authors declare no competing financial interest.

■ REFERENCES

(1) Barnes, H. A. Shear-Thickening ("Dilatancy") in Suspensions of Nonaggregating Solid Particles Dispersed in Newtonian Liquids. *J. Rheol.* **1999**, *33*, 329−366.

(2) Wagner, N. J.; Brady, J. F. Shear Thickening in Colloidal Dispersions. *Phys. Today* **2009**, *62*, 27−32.

(3) Brown, E.; Jaeger, H. M. Shear Thickening in Concentrated Suspensions: Phenomenology, Mechanisms and Relations to Jamming. *Rep. Prog. Phys.* **2014**, *77*, 046602.

(4) Mewis, J.; Wagner, N. J. *Colloidal Suspension Rheology*; Cambridge University Press: Cambridge, U.K., 2013.

(5) Lee, Y. S.; Wetzel, E. D.; Wagner, N. J. The Ballistic Impact Characteristics of Kevlar® Woven Fabrics Impregnated with a Colloidal Shear Thickening Fluid. *J. Mater. Sci.* **2003**, *38*, 2825−2833.

(6) Fischer, C.; Braun, S. A.; Bourban, P.-E.; Michaud, V.; Plummer, C. J. G.; Månson, J. -a. E. Dynamic Properties of Sandwich Structures with Integrated Shear-Thickening Fluids. *Smart Mater. Struct.* **2006**, *15*, 1467−1475.

(7) Warren, J.; Cole, M.; Offenberger, S.; Lacy, T. E.; Toghiani, H.; Burchell, M.; Kundu, S.; Pittman, C. U. Hypervelocity Impact of Honeycomb Core Sandwich Panels Filled with Shear Thickening Fluid. *28th Technical Conference of the American Society for Composites*, State College, PA, Sept 9−11, 2013; Destech Publications: Lancaster, PA, 2013; pp 124−135.

(8) Boersma, W. H.; Laven, J.; Stein, H. N. Shear Thickening (dilatancy) in Concentrated Dispersions. *AIChE J.* **1990**, *36*, 321−332.

(9) Mewis, J.; Biebaut, G. Shear Thickening in Steady and Superposition Flows Effect of Particle Interaction Forces. *J. Rheol.* **2001**, *45*, 799.

(10) Liu, X.-Q.; Bao, R.-Y.; Wu, X.-J.; Yang, W.; Xie, B.-H.; Yang, M.-B. Temperature Induced Gelation Transition of a Fumed silica/PEG Shear Thickening Fluid. *RSC Adv.* **2015**, *5*, 18367−18374.

(11) Hoffman, R. L. Discontinuous and Dilatant Viscosity Behavior in Concentrated Suspensions. I. Observation of a Flow Instability. *J. Rheol.* **1972**, *16*, 155−173.

(12) Hoffman, R. L. Discontinuous and Dilatant Viscosity Behavior in Concentrated Suspensions. II. Theory and Experimental Tests. *J. Colloid Interface Sci.* **1974**, *46*, 491−506.

(13) Foss, D. R.; Brady, J. F. Structure, Diffusion and Rheology of Brownian Suspensions by Stokesian Dynamics Simulation. *J. Fluid Mech.* **2000**, *407*, 167−200.

(14) Kalman, D. P.; Wagner, N. J. Microstructure of Shear-Thickening Concentrated Suspensions Determined by Flow-USANS. *Rheol. Acta* **2009**, *48*, 897−908.

(15) Cheng, X.; McCoy, J. H.; Israelachvili, J. N.; Cohen, I. Imaging the Microscopic Structure of Shear Thinning and Thickening Colloidal Suspensions. *Science* **2011**, *333*, 1276−1279.

(16) Mari, R.; Seto, R.; Morris, J. F.; Denn, M. M. Shear Thickening, Frictionless and Frictional Rheologies in Non-Brownian Suspensions. *J. Rheol.* **2014**, *58*, 1693−1724.

(17) Fernandez, N.; Mani, R.; Rinaldi, D.; Kadau, D.; Mosquet, M.; Lombois-Burger, H.; Cayer-Barrioz, J.; Herrmann, H. J.; Spencer, N. D.; Isa, L. Microscopic Mechanism for Shear Thickening of Non-Brownian Suspensions. *Phys. Rev. Lett.* **2013**, *111*, 108301.

(18) Heussinger, C. Shear Thickening in Granular Suspensions: Interparticle Friction and Dynamically Correlated Clusters. *Phys. Rev. E* **2013**, *88*, 050201.

(19) Seto, R.; Mari, R.; Morris, J. F.; Denn, M. M. Discontinuous Shear Thickening of Frictional Hard-Sphere Suspensions. *Phys. Rev. Lett.* **2013**, *111*, 218301.

(20) Lootens, D.; van Damme, H.; Hémar, Y.; Hébraud, P. Dilatant Flow of Concentrated Suspensions of Rough Particles. *Phys. Rev. Lett.* **2005**, *95*, 268302.

(21) Wyart, M.; Cates, M. E. Discontinuous Shear Thickening without Inertia in Dense Non-Brownian Suspensions. *Phys. Rev. Lett.* **2014**, *112*, 098302.

(22) Van de Ven, T. G. M. *Colloidal Hydrodynamics*; Academic Press: London, 1989.

(23) Iskakova, L. Y.; Zubarev, A. Y. Shear Thickening of Dense Suspensions due to Energy Dissipation in Lubrication Layers between Particles. *Phys. Rev. E* **2013**, *88*, 032303.

(24) Zhao, Y.; Davis, R. H. Interaction of Two Touching Spheres in a Viscous Fluid. *Chem. Eng. Sci.* **2002**, *57*, 1997−2006.

(25) Chellamuthu, M.; Arndt, E. M.; Rothstein, J. P. Extensional Rheology of Shear-Thickening Nanoparticle Suspensions. *Soft Matter* **2009**, *5*, 2117−2124.

(26) Raghavan, S. R.; Walls, H. J.; Khan, S. A. Rheology of Silica Dispersions in Organic Liquids: New Evidence for Solvation Forces Dictated by Hydrogen Bonding. *Langmuir* **2000**, *16*, 7920−7930.

(27) Raghavan, S. R.; Khan, S. A. Shear-Thickening Response of Fumed Silica Suspensions under Steady and Oscillatory Shear. *J. Colloid Interface Sci.* **1997**, *185*, 57−67.

(28) Negi, A. S.; Osuji, C. O. New Insights on Fumed Colloidal Rheology—shear Thickening and Vorticity-Aligned Structures in Flocculating Dispersions. *Rheol. Acta* **2009**, *48*, 871−881.

(29) Crawford, N. C.; Williams, S. K. R.; Boldridge, D.; Liberatore, M. W. Shear-Induced Structures and Thickening in Fumed Silica Slurries. *Langmuir* **2013**, *29*, 12915−12923.

(30) Barthel, H.; Rösch, L.; Weis, J. Fumed Silica-Production, Properties, and Applications. *Organosilicon Chem. Set Mol. Mater.* **1996**, 761−778.

(31) Mathias, J.; Wannemacher, G. Basic Characteristics and Applications of Aerosil: 30. The Chemistry and Physics of the Aerosil Surface. *J. Colloid Interface Sci.* **1988**, *125*, 61−68.

(32) *Technical Bulletin Fine Particles 11: Basic Characteristics of AEROSIL® Fumed Silica*; Evonik Industries: Cincinnati, OH, 2006.

(33) O'Brie, V. T.; Mackay, M. E. Stress Components and Shear Thickening of Concentrated Hard Sphere Suspensions. *Langmuir* **2000**, *16*, 7931−7938.

(34) Jiang, T.; Zukoski, C. F. Role of Particle Size and Polymer Length in Rheology of Colloid−Polymer Composites. *Macromolecules* **2012**, *45*, 9791−9803.

(35) Glomann, T.; Hamm, A.; Allgaier, J.; Hübner, E. G.; Radulescu, A.; Farago, B.; Schneider, G. J. A Microscopic View on the Large Scale Chain Dynamics in Nanocomposites with Attractive Interactions. *Soft Matter* **2013**, *9*, 10559−10571.

(36) Kim, S. Y.; Meyer, H. W.; Saalwächter, K.; Zukoski, C. F. Polymer Dynamics in PEG-Silica Nanocomposites: Effects of Polymer Molecular Weight, Temperature and Solvent Dilution. *Macromolecules* **2012**, *45*, 4225−4237.

(37) Kumar, S. K.; Jouault, N.; Benicewicz, B.; Neely, T. Nanocomposites with Polymer Grafted Nanoparticles. *Macromolecules* **2013**, *46*, 3199−3214.

DOI: 10.1021/acsami.5b05094
ACS Appl. Mater. Interfaces 2015, 7, 18650−18661

(38) Rubenstein, M.; Colby, R. H. *Polymer Physics*; Oxford University Press: New York, 2003.
(39) He, L.; Hu, Y.; Wang, M.; Yin, Y. Determination of Solvation Layer Thickness by a Magnetophotonic Approach. *ACS Nano* **2012**, *6*, 4196−4202.
(40) Guazzelli, É.; Morris, J. F. *A Physical Introduction to Suspension Dynamics*, 1st ed.; Cambridge University Press: Cambridge, U.K., 2012.
(41) Kim, S.; Karrila, S. J. *Microhydrodynamics: Principles and Selected Applications*, unabridged ed.; Dover Publications: Mineola, NY, 2005.
(42) Frankel, N. A.; Acrivos, A. On the Viscosity of a Concentrated Suspension of Solid Spheres. *Chem. Eng. Sci.* **1967**, *22*, 847−853.
(43) Vincent, B.; Edwards, J.; Emmett, S.; Jones, A. Depletion Flocculation in Dispersions of Sterically-Stabilised Particles ("soft Spheres"). *Colloids Surf.* **1986**, *18*, 261−281.
(44) Jiang, W.; Gong, X.; Xu, Y.; Xuan, S.; Jiang, W.; Zhu, W.; Li, X.; Qin, L. Investigating the Confining Compressibility of STF at High Deformation Rate. *Eur. Phys. J.: Appl. Phys.* **2012**, *60*, 31101.
(45) Maranzano, B. J.; Wagner, N. J. Thermodynamic Properties and Rheology of Sterically Stabilized Colloidal Dispersions. *Rheol. Acta* **2000**, *39*, 483−494.

DOI: 10.1021/acsami.5b05094
ACS Appl. Mater. Interfaces 2015, 7, 18650−18661